



Deposited via The University of Sheffield.

White Rose Research Online URL for this paper:

<https://eprints.whiterose.ac.uk/id/eprint/150794/>

Version: Accepted Version

---

**Article:**

Smyl, D. and Liu, D. (2019) Invisibility and indistinguishability in structural damage tomography. *Measurement Science and Technology*, 31 (2). 024001. ISSN: 0957-0233

<https://doi.org/10.1088/1361-6501/ab43f2>

---

Article available under the terms of the CC-BY-NC-ND licence  
(<https://creativecommons.org/licenses/by-nc-nd/3.0/>).

**Reuse**

This article is distributed under the terms of the Creative Commons Attribution-NonCommercial-NoDerivs (CC BY-NC-ND) licence. This licence only allows you to download this work and share it with others as long as you credit the authors, but you can't change the article in any way or use it commercially. More information and the full terms of the licence here: <https://creativecommons.org/licenses/>

**Takedown**

If you consider content in White Rose Research Online to be in breach of UK law, please notify us by emailing [eprints@whiterose.ac.uk](mailto:eprints@whiterose.ac.uk) including the URL of the record and the reason for the withdrawal request.

# Invisibility and indistinguishability in structural damage tomography

Danny Smyl<sup>1,2</sup>

<sup>1</sup>Department of Civil and Structural Engineering, The University of Sheffield, Sheffield, UK

<sup>2</sup>The Integrated Civil and Infrastructure Research Centre (ICAIR), Sheffield, UK

E-mail: d.smyl@sheffield.ac.uk

Dong Liu<sup>2,3,4</sup>

<sup>3</sup>Hefei National Laboratory for Physical Sciences at the Microscale and Department of Modern Physics, University of Science and Technology of China, Hefei 230026, China

<sup>4</sup>CAS Key Laboratory of Microscale Magnetic Resonance, University of Science and Technology of China, Hefei 230026, China

<sup>5</sup>Synergetic Innovation Center of Quantum Information and Quantum Physics, University of Science and Technology of China, Hefei 230026, China

E-mail: dong2016@ustc.edu.cn

**Abstract.** Structural damage tomography (SDT) uses full-field or distributed measurements collected from sensors or self-sensing materials to reconstruct quantitative images of potential damage in structures, such as civil structures, automobiles, aircraft, etc. In approximately the past ten years, SDT has increased in popularity due to significant gains in computing power, improvements in sensor quality, and increases in measurement device sensitivity. Nonetheless, from a mathematical standpoint, SDT remains challenging because the reconstruction problems are usually nonlinear and ill-posed. Inasmuch, the ability to reliably reconstruct or detect damage using SDT is seldom guaranteed due to factors such as noise, modeling errors, low sensor quality, and more. As such, damage processes may be rendered invisible due to data indistinguishability. In this paper we identify and address key physical, mathematical, and practical factors that may result in invisible structural damage. Demonstrations of damage invisibility and data indistinguishability in SDT are provided using experimental data generated from a damaged reinforced concrete beam.

*Keywords:* Electrical resistance tomography, inverse problems, nondestructive evaluation, structural health monitoring, tomography

## 1. Introduction

Structural damage tomography (SDT) utilizes full-field or distributed measurements from area/point sensors or self-sensing materials (i.e. carbon-based [1, 2], cement-based [3], etc.) to reconstruct 2- or 3D tomographic images of potential damage. SDT has gained significant

traction over the past ten years in the fields of nondestructive testing (NDT) and structural health monitoring (SHM), much of this owing to gains in computing power, improvements in sensor quality, and increased sensitivity of measurement devices [4]. Moreover, numerous stationary and non-stationary modalities have been used, such as electrical resistance tomography (ERT) [5, 6, 7], electrical-based enclosure methods [8], guided wave based tomography [9, 10], elasticity imaging [11, 12], and digital image correlation [13, 14]. Most commonly, reconstructions generated by these imaging modalities are computed by solving an inverse problem. The inverse problems are generally nonlinear and ill-posed, broadly meaning that the parameters reconstructed  $\theta$  are highly sensitive to changes in the input data  $d$ . It is therefore clear that even small sources of error in  $d$ , such as corrupting noise, have a significant impacts on  $\theta$ . To examine this further, we write down the typical observation model for a damage tomography problem as

$$d = U(\theta) + e \quad (1)$$

where  $U(\theta)$  is a numerical model and  $e$  is an additive error term. As an overarching statement, the general aim of a single-state SDT inverse problem is to match the left and right hand sides of Eq. 1 as closely as tolerably possible. As an intuitively appealing extension, one may immediately ask: How large can  $e$  be before SDT reconstructions are no longer reliable?

This question is not well understood in current SDT literature [4] and is a central theme of this article. However, in addressing this query, we must first recognize that (typically<sup>‡</sup>) in order to asses damage, we require the comparison of two states, as noted in the second axiom of SHM [17]:

“Axiom II: The assessment of damage requires a comparison between two system states.”

Based on this realization, consider parameter fields  $\theta_u$  and  $\theta_d$  corresponding to undamaged (subscript u) and damaged states (subscript d), respectively. Accordingly, we also have measured data  $d_u$  and  $d_d$ . Informally, it is apparent that states  $\theta_u$  and  $\theta_d$  are only distinguishable if  $d_u - d_d$  is above some threshold  $e_t$ , i.e.  $d_u - d_d > e_t$ . In other words, when  $d_u - d_d < e_t$ , potential damage contained in  $\theta_d$  is *invisible due to indistinguishable measurements*  $d_u$  and  $d_d$ .

Quite possibly, the first formal distinguishability criterion was derived by Isaacson [18]. In this seminal work, Isaacson found that two parameter fields were distinguishable, in the least squares sense, when the following criteria is met

$$||d_1(\theta_1) - d_2(\theta_2)|| > e_p \quad (2)$$

<sup>‡</sup> Other methods for damage tomography using only one data set, such as baseline-free methods [15, 16], have also proven successful. Definitions of invisibility and indistinguishability in such contexts will be defined in later work.

where  $d_1$  and  $d_2$  are data corresponding to parameters  $\theta_1$  and  $\theta_2$  and  $e_p > 0$  was surmised to be the measurement precision. In the original work, Isaacson studied the distinguishability of two conductivity fields in the context of ERT. While the original work was only applied to ERT, the criterion in Eq. 2 has provided fundamental insight into the “reconstructability” of many other inverse problems [19, 20, 21, 22, 23] as well as optimization of measurement schemes [24, 25]. In cases where measurement noise is the prevailing factor in reconstruction quality, Eq. 2 is an excellent criteria for distinguishability.

In SDT, however, measurement precision, as it relates to noise, is often not the only (or even primary) factor affecting the distinguishability of data sets and therefore the visibility/invisibility of damage interpreted from  $\theta_d$ . In many cases, SDT data is taken from large structures that are inhomogeneous in material constitution, highly nonlinear, have uncertain boundary conditions, and have highly localized damage that is small relative to the structure/sensor size, etc. Moreover, due to their large size and environmental exposure, sensor properties often vary both spatially and temporally [26]. The combination of these factors, and others, create challenging modeling conditions (i.e. decreasing the accuracy of  $U$ ), testing conditions, and add uncertainties into SDT inverse problems [27]. As such, the classic distinguishability criteria in Eq. 2 is insufficient for many SDT applications.

At present, indistinguishability and damage invisibility are not well understood in the context of SDT. In this work, we aim to bridge this gap in knowledge. We begin by developing a new distinguishability model and damage visibility criterion for SDT, including components relevant to practical applications. Based on this model, we then use experimental data to demonstrate damage invisibility resulting from data indistinguishability in the context of an emerging SDT imaging modality: ERT. Following, discussion and conclusions are provided.

## 2. A distinguishability model for damage tomography and the visibility criterion

In this section, we first derive a general model for distinguishability in SDT and discuss the contributing factors. Following, we clearly define the SDT damage visibility criterion. We begin by writing the observation models for both undamaged and damaged states

$$\begin{aligned} d_u &= U(\theta_u) + e_u \\ d_d &= U(\theta_d) + e_d \end{aligned} \tag{3}$$

where  $e_u$  and  $e_d$  are the error terms for the undamaged and damaged states, respectively. We then substitute observation model data sets into Eq. 2 as follows

$$e_p < ||d_u - d_d|| \tag{4}$$

where we assume that  $e_p$  is a sufficient lower bound for data distinguishability in SDT – which is a reasonable assumption given the low noise floor of many contemporary SDT electronic measuring systems [28]. We now add an additional term to this inequality by writing

$$e_p < \|d_u - d_d\| < e_{\text{SDT}} \quad (5)$$

where  $e_{\text{SDT}}$  is an upper bound on data distinguishability. The physical interpretation of the upper bound  $e_{\text{SDT}}$  is related to the maximum feasible distance between vectors  $d_u$  and  $d_d$  measured here with the Euclidean norm. In the purest sense, it is certainly true that – for a *fixed* degree of damage – even when the data difference  $d_u - d_d$  is exceedingly high as a result of SDT errors *alone*, the information contained in  $d_d$  may indeed be visible (in the sense that  $\theta_d$  may be reconstructed). However, for such a fixed degree of damage, when the auxiliary errors dominate or behave as the main error source, to distinguish  $\theta_d$  from  $\theta_u$ , an upper constraint is required in Eq. 5. From a pragmatic SHM viewpoint, this means that when  $\|d_u - d_d\| > e_{\text{SDT}}$ , assessment of damage via SHM Axiom II is not meaningful.

It is important to remark here that the data difference term  $\|d_u - d_d\|$  is merely a mechanism for assessing SDT errors intrinsic in  $d_u$  and  $d_d$ . Specifically, we are interested in the auxiliary errors present in the data, ultimately resulting in data distinguishability/indistinguishability. Nonetheless, the use of  $\|d_u - d_d\|$  is practical because decoupling and *exactly* quantifying all sources of SDT errors in  $d_u$  and  $d_d$  is not possible since there are an infinite number of SDT conditions, physical environments, geometries, sensors, etc.

Nonetheless, we are often interested in approximating the aforementioned errors [29]. In doing this, we may reformulate Eq. 5 by substituting  $d_u$  and  $d_d$  from Eq. 3 into Eq. 5 to obtain

$$e_p < \|U(\theta_u) + e_u - U(\theta_d) - e_d\| < e_{\text{SDT}} \quad (6)$$

which can be rearranged into a more compact expression

$$e_p < \|U(\theta_u) - U(\theta_d) + e_c\| < e_{\text{SDT}} \quad (7)$$

by combining the error terms, i.e.  $e_c = e_u - e_d$ . The SDT distinguishability criterion is now given by the equivalent expressions in Eq. 5 and Eq. 7, where the error term  $e_c$  encapsulates the prevalent SDT errors due to noise,  $e_n$ , numerical modeling errors  $e_m$ , discretization errors  $e_d$ , interpolation errors  $e_I$ , and errors resulting from sensor quality  $e_s$ . In other words  $e_c \approx e_n + e_m + e_d + e_I + e_s$ , which clearly indicates that the SDT upper bound on distinguishability is much larger than the measurement precision alone, i.e.  $e_{\text{SDT}} \gg e_p$ §. We therefore expect an overall lower likelihood of visible damage(s) potentially present in  $\theta_d$  than if measurement precision, alone, was responsible for data distinguishability. Further, we note that the symbol ‘ $\approx$ ’ is used because there are other sources of error of secondary importance, such as computational round off errors [30]. For completeness, we describe the major components of error in SDT and important resulting considerations in the following.

**Error due to random noise,  $e_n$ :** Random noise has a direct influence on measurement accuracy and precision. For SDT applications, we define measurement accuracy as the closeness of

§ An intrinsic assumption in the additive error model  $e_c = e_c(\cdot)$  is that all sources of errors are independent.

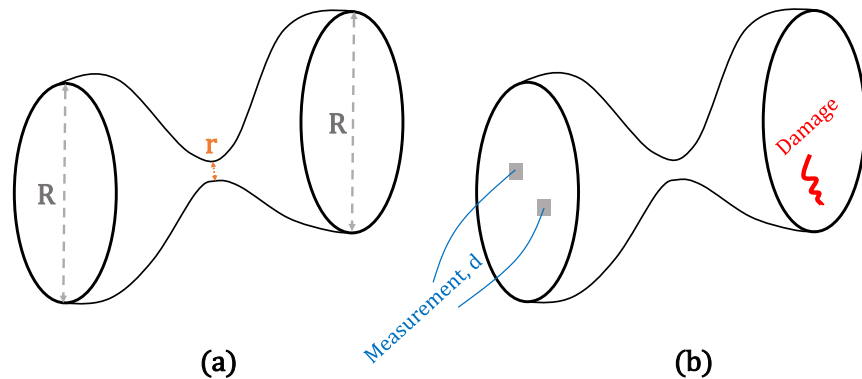


**Figure 1.** Schematic manifold example demonstrating the effect of geometry on the visibility of damage. Schematics, (a) contracted cylinder with end radii  $R$  and constricted radius  $r$  and (b) damaged geometry with left hand side local boundary measurements  $d$  and right hand side damage. As  $r \rightarrow 0$ , a singularity is formed and the damage inferred from  $d$  is invisible.

a measurement to the true value, while measurement precision is the repeatability of a measurement. As a first-order thought experiment, it is often assumed that when all other sources of error are zero and  $e_n = 0$ , a solution to a SDT inverse problem is viable. This is because the signal  $d$  to noise ratio tends to infinity; i.e. as  $e_n \rightarrow 0$ ,  $d/e_n \rightarrow \infty$ . While this assumption is often reasonable for simple applications of SDT, the general case is more complicated [31]. Take for example the geometry shown in Fig. 1a, where two parts of a constricted cylinder (large radius  $R$ ) are connected by a constricted area (small radius  $r$ ). It is obvious that as  $r \rightarrow 0$  a singularity develops at the location of the constriction. Therefore, in the example case shown in Fig 1b, as  $r \rightarrow 0$  the damage (right hand side) inferred by local boundary measurements (left hand side) becomes invisible. Moreover, it is apparent that the visibility of the damage is dependent on  $R/r$  resulting from the accuracy and precision of measurement  $d = d(R/r)$ . As such, if  $e_n$  is present in  $d$ , i.e. if  $d = d(R/r, e_n)$ , the damage becomes invisible at a relatively higher radius  $r$  (or, alternatively at a lower  $R/r$ ) than if  $e_n$  was not present. We therefore infer that the visibility of a damage process is directly linked to  $e_n$  and the SDT geometry.

**Numerical modeling errors,  $e_m$ :** Every numerical model has error [32]. In the case of the finite element method (FEM), which is possibly the most popular numerical method employed in SDT, it is well known that FEM solutions converge exponentially with the simultaneous refinement of discretization size  $h$  and increase of interpolation polynomial order  $p$  [33, 34, 35]. In reality,  $h = 0$  and  $p = \infty$  is impossible, so we must live with a non-zero  $e_m$ . The severity of  $e_m$  is directly linked to the accuracy of the numerical model. In SDT cases where the material constitution is heterogeneous or highly non-linear, one can expect an increase in  $e_m$  relative to, e.g. an isotropic linear constitution [36]. In addition,  $e_m$  may also include errors due to uncertainty in source terms or boundary conditions, factors that commonly contribute to errors in SDT [4].

**Discretization errors,  $e_d$ :** When SDT approaches are formulated such that a continuous model with an infinite-dimensional space  $\Omega$  is discretized to  $\Omega_h$  – a practical requirement – discretization error occurs [37]. Since convergence of, e.g. the FEM, is guaranteed as  $h \rightarrow 0$ , it is therefore expected that coarse discretizations (large  $h$ ) have more discretization error than finer discretizations. This reality is ever present in large inverse problems as representing  $\Omega_h$  with an ultra-fine  $h$  results in significant computational demand. Due to the significance of  $e_d$  in inverse

problems, works such as [37] have developed Bayesian Approximative Error (BAE) approaches for dealing with  $e_d$ . In fact,  $e_d$  and  $e_m$  may be lumped in the same error model using BAE [38].

**Interpolation errors,  $e_I$ :** Interpolation errors in SDT result from situations where a measured data field is interpolated onto a mesh. The severity of interpolation errors scales with the accuracy of the interpolation method. For example, in 2D cases where over fitting is not expected, interpolation schemes ranging from lowest to highest accuracy would be: nearest neighbor  $\rightarrow$  bi-linear  $\rightarrow$  bi-quadratic  $\rightarrow \dots$ . In SDT, interpolation errors are prevalent in, e.g. elasticity imaging [11] and FEM-based digital image correlation [39].

**Errors resulting from sensor quality,  $e_s$ :** There are many sources of systematic and random errors in point and area sensors. Error sources range from inhomogeneous distributions in area sensor thickness [27] to quantum deviations in optical sensors [40]. While much of the sensor error may be mitigated with quality control [41], some sources of error related to sensor quality may be difficult to avoid, such as contemporary limitations in manufacturing [42] or quantum factors [43].

With error sources and mathematical preliminaries provided, we now define the criteria used in solving SDT visibility problem: is damage inferred from  $\theta_d$  visible with respect to  $\theta_u$ ? The question is shown schematically in Fig. 2. The solution to the SDT visibility problem hinges on whether or not the distinguishability criteria (Eqs. 5 or 7) between data from damaged and undamaged states is met. In other words, for a specific SDT application (fixed geometry, sensor type, measurement scheme, numerical model, and time of measurement), damage is invisible when the following is satisfied:

$$\text{Damage invisibility criterion: } \|U(\theta_u) - U(\theta_d) + e_c\| < e_p \text{ or } \|U(\theta_u) - U(\theta_d) + e_c\| > e_{SDT}.$$

Conversely, damage is visible when the following is satisfied:

$$\text{Damage visibility criterion: } e_p < \|U(\theta_u) - U(\theta_d) + e_c\| < e_{SDT}.$$

We remark that a number of equivalent useful statements may also be written by substituting expressions from Eq. 3.

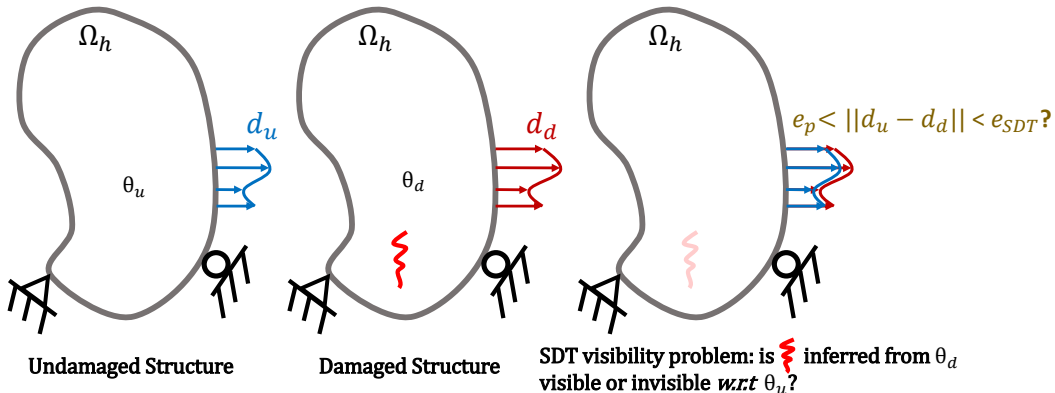


**Figure 2.** Schematic representation of the SDT visibility problem. Left column, a discretized undamaged structure with measured data  $d_u$ ; middle column, a discretized damaged structure with measured data  $d_d$  (damage depicted as a red sig-zag); right column, an illustration of the SDT visibility problem.

At this point, we have established criteria for damage visibility and data distinguishability. However, while  $e_p$  can be measured using straightforward experimental measurements, the value of the scalar  $e_{\text{SDT}}$  is not numerically defined. This is because  $e_{\text{SDT}}$  is unique for a given problem, and it must therefore be computed on a case-by-case basis. One possible regime for estimating  $e_{\text{SDT}}$ , among other possible methods, would be to use of a goodness of fit measure between reconstructions of  $\theta_u$  and  $\theta_d$ . For example, one could take advantage of the Pearson correlation coefficient (PCC), where  $\text{PCC}(\theta_u, \theta_d) = 0$  (linearly uncorrelated) when the following criterion is met

$$\|U(\theta_u) - U(\theta_d) + e_c\| = e_{\text{SDT}}. \quad (8)$$

There are many ways in one may optimize Eq. 8 computationally such that  $\text{PCC}(\theta_u, \theta_d) \approx 0$ . For example, one could conduct simulations for ground truth distributions  $\theta_u$  and  $\theta_d$  and iterate over random Gaussian distributions or summing random distributions for  $e_c$  with an objective function aiming to reach  $\text{PCC}(\theta_u, \theta_d) = 0$ . It is important to note here that, for SDT problems in general,  $e_{\text{SDT}} \in (e_p, \infty)$  since a given SDT problem can consist of a data set with arbitrary size, noise corruption, and/or a numerical model with arbitrary modeling error. However, to these ends, since the aim of this work is primarily to present the SDT distinguishability model, the visibility criterion, and provide relevant examples of damage invisibility, we defer the presentation of advanced regimes for computing  $e_{\text{SDT}}$  to future work.

### 3. Structural damage invisibility in ERT

In this section, we provide examples of damage invisibility/visibility using an emerging SDT imaging modality: ERT. We begin by detailing the ERT inverse problem and solution regime. Following, we (i) demonstrate damage invisibility and data indistinguishability and (ii) approximate  $e_{\text{SDT}}$  using experimental data generated from a damaged reinforced concrete member with an applied sensing skin. Lastly, a brief discussion is provided.

#### 3.1. Damage invisibility in ERT

In this work, we aim to reconstruct a crack in an area sensor painted atop a reinforced concrete beam element. For this, we utilize ERT, which is a diffusive imaging modality where we aim to reconstruct the electrical conductivity  $\sigma$  from electric potential measurements  $V$  [44, 45]. The resulting observation model for this problem is written as

$$V = U(\sigma) + e_{\text{ERT}} \quad (9)$$

where  $e_{\text{ERT}}$  is the additive ERT error term. For  $U(\sigma)$ , we utilize the complete electrode model (CEM) discretized using the FEM. For further details related to the numerical implementation of the CEM, we refer the reader to [3, 46]. Resulting from Eq. 9, we have a one-state least squares optimization problem where we aim to minimize the functional

$$\Psi_{\text{ERT}}(\sigma > 0) = \|L_e(V - U(\sigma))\|^2 + R_\sigma(\sigma) \quad (10)$$

where  $L_e$  is the Cholesky factorization of the inverse noise covariance matrix  $W^{-1}$  (i.e.  $L_e^T L_e = W^{-1}$ ) and  $R_\sigma(\sigma)$  is a regularization term that incorporates prior information and adds stability to the otherwise non-unique and ill-posed problem in Eq. 10. In order to estimate the contact impedances, we computed the (assumed) homogeneous impedances  $z_{\text{hom}}$  simultaneously with the

best homogeneous estimate of the conductivity  $\sigma_{\text{hom}}$ . To do this, we solved the following two-parameter minimization problem:  $(\sigma_{\text{hom}}, z_{\text{hom}}) = \text{argmin}\{\|V_u - U(\sigma, z)\|^2\}$  where  $\sigma_{\text{hom}}$  was also used as the initial guess for  $\sigma$ . Since we are interested in reconstructing cracks, we utilize total variation (TV) regularization, which is well-known for its edge-preserving characteristics [47] and well-suited for crack detection in SDT [27]. Moreover, we utilize the interior point method with second-order polynomial barrier functions in the constrained optimization of  $\Psi_{\text{ERT}}(\sigma > 0)$ . For solving the optimization problem, we utilize a Gauss-Newton regime equipped with a line search as described in [4]. In the following, this ERT regime will be implemented in a case study investigating the visibility/invisibility of a small crack in a concrete beam.

### 3.2. Case study: Visibility and invisibility of a small crack in a concrete beam imaged with ERT

In this case study, we investigate the visibility of a qualitatively small crack generated by mechanically loading a  $152 \times 508 \times 152$  mm lightly-reinforced concrete beam in 3-point bending (full experimental details provided in [4]). A photograph of the beam and sensing skin are shown in Fig. 3. To image the concrete beam using ERT, a rectangular electrically conductive silver sensing skin was painted atop 28 boundary electrodes affixed to the beam surface. In the measurement program, 54 DC injections with an amplitude of 1 mA were applied between electrodes  $i$  and  $j$ ,  $i = 6, 21$  and  $j = 1, \dots, 28, i \neq j$ . For each current injection, a total of 1,458 adjacent electrode potentials measurements were taken. The measurements were taken from an in-house system consisting of a power supply, 32-channel switch (28 channels used here), and a PC equipped with a Java code to execute the ERT measurements. Moreover, the channel-wise SNR of the system was, on average, 63 dB using repeated measurements. In solving the numerical forward model  $U(\sigma)$ , we used an unstructured rectangular FEM mesh with  $N_{el} = 2,572$  triangular elements and  $N_n = 1,406$  nodes.

We note that, in the experimental program, measurements from cracking patterns ranging from one barely visible crack to multiple large cracks were taken. While the ability of ERT to reconstruct large complex cracking patterns was confirmed in [48], this theme is not the focus of this work. Rather, we are more interested in investigating the visibility of small damages, where the difference between the undamaged measurement  $V_u$  and damaged measurement  $V_d$  is smallest. In other words,  $\|V_u - V_d\|$  is the lowest and therefore the measurements have a higher likelihood of being indistinguishable than in cases with higher cracking. As such, we study the visibility/invisibility of the smallest visible crack visible by eye on the sensing skin during the loading process. The highlighted crack is shown in the top row of Fig. 3.

In the data analysis, it was found that the potential measurements corresponding to the small crack case were well within the distinguishability range, i.e.  $e_p < \|V_u - V_d\| < e_{\text{SDT}}$ . Therefore, the crack was visible in the ERT reconstruction, as demonstrated in Fig 3a. Therefore, to test the visibility of the crack in a suite of cases with increasing errors, we introduce errors into the forward model term  $U(\sigma)$  by rewriting Eq. 5 as  $e_p < \|V_u - U(\sigma) + e_c\| < e_{\text{SDT}}$ . Through this substitution, we may add modeling errors directly into the forward problem  $U(\sigma)$  in addition to adding noise into  $V_u$ . For this, progressively increasing modeling error was added to  $U$  by adding random horizontal and vertical perturbations  $\Delta_{el}$  to the center locations of the top/bottom electrodes and side electrodes, respectively. The maximum magnitude of the perturbations was within the range of  $1.0 \leq \Delta_{el} \leq 6.0\%$  of the electrode widths. In addition, 2.0% noise standard deviation was added to the contact impedances  $\eta_z$  and undamaged potential measurements  $\eta_V$  (i.e.  $V_u = V_u + \eta_V$ ). This

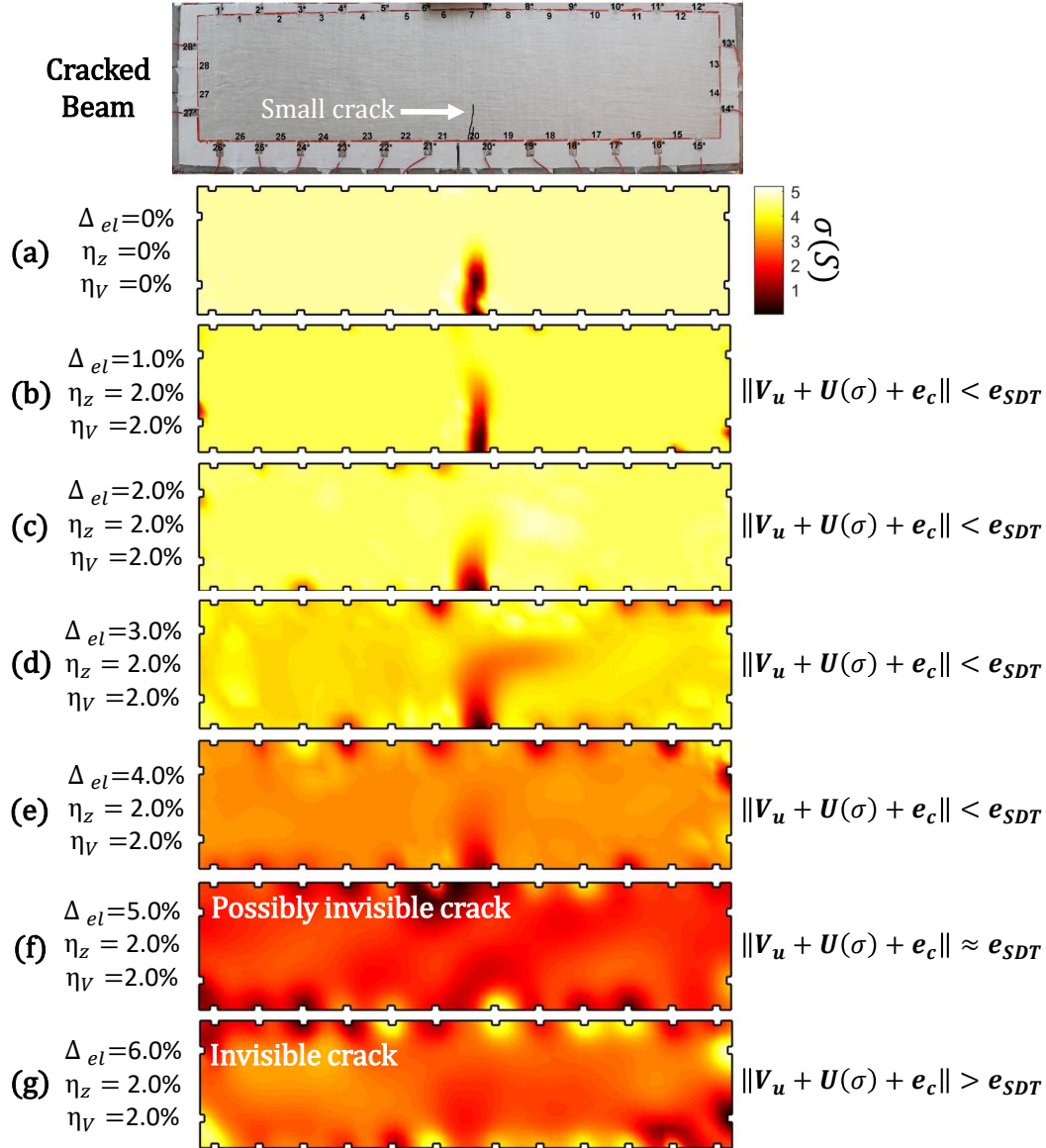


**Figure 3.** ERT reconstructions of a small crack in a sensing skin painted on a concrete beam element demonstrating the effect of noise and model error or crack visibility. Top row, a photograph of the concrete beam, sensing skin, and electrode numbers. Row (a) reconstruction of the small crack without added modeling error via perturbations in electrode location  $\Delta_{el}$  or noise added to the potential measurements  $\eta_V$  and contact impedances  $\eta_z$ . Rows (b) - (g), reconstructions with the addition of  $\Delta_{el}$ ,  $\eta_V$ , and  $\eta_z$ .

level of added noise was selected since it is likely on the high-end of realistic noise levels for low temporal resolution SDT-ERT imaging. It was therefore intrinsically assumed that modeling errors (due to sensor flaws/electrode perturbations) are the dominating culprit for damage invisibility in this SDT application of ERT. The reconstructions with additional modeling error  $e_m$  and random noise  $e_n$ , which are cumulative in  $e_c$ , are shown in Fig. 3b-g.

Based on visual observation of reconstructions shown in Fig. 3, the central cracks in

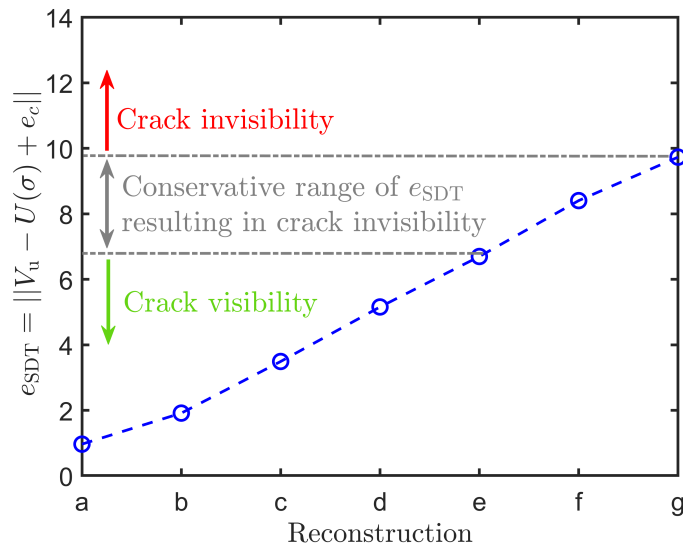


**Figure 4.** Upper distinguishability threshold  $e_{\text{SDT}}$  for the ERT case study plotted against reconstructions (a) - (g) having increasing modeling errors induced through perturbations in electrode location  $\Delta_{el}$  ranging from 0% to 6% in reconstructions (a) and (g), respectively. The conservative range of  $e_{\text{SDT}}$  resulting in crack invisibility is indicated by the space between the dotted horizontal lines. The regions above and below the horizontal lines are regions of crack invisibility and visibility, respectively.

reconstructions (b)-(e) are visible via the local reduction in  $\sigma$ . The visibility of the cracks clearly fade proportional to the magnitude of modeling error induced by  $\Delta_{el}$ , to the point that the crack in reconstruction (e) is barely visible. This indicates that data used in (e) is marginally below the distinguishability threshold  $e_{\text{SDT}}$ . On the other hand, in reconstruction (f), it is not clear whether or not the crack is visible or if the locally reduced conductivity in the center is a reconstruction artifact. Moreover, there are significant artifacts in the background  $\sigma$  of reconstruction (f); as such, we may surmise that data used in reconstruction (f) is near the upper distinguishability threshold, i.e.  $\|V_u - U(\sigma) + e_c\| \approx e_{\text{SDT}}$ . In the final reconstruction, (g), the crack is invisible and we therefore conclude that data used in this reconstruction has surpassed  $e_{\text{SDT}}$ .

From these results, we can approximate the range of  $e_{\text{SDT}}$  resulting in crack invisibility. To do this, we conservatively assume that the crack becomes invisible when  $\Delta_{el} > 4.0\%$ . Put differently, we can assume cracks in reconstructions (f) and (g) are invisible and therefore the input data are indistinguishable at some point after reconstruction (e). The resulting range of  $e_{\text{SDT}}$  can be depicted graphically by plotting  $\|V_u - U(\sigma) + e_c\|$  against reconstructions (a) - (g) as shown in Fig. 4. Based on these assumptions, we find the conservative bounds of  $e_{\text{SDT}}$  resulting in crack invisibility to lie approximately within the range  $6.5 < e_{\text{SDT}} < 9.75$ . Therefore, for this case, we may conclude that when  $9.75 < \|V_u - U(\sigma) + e_c\|$ , cracks are invisible. In contrast, when  $e_p < \|V_u - U(\sigma) + e_c\| < 6.5$ , we may conclude that cracks are visible.

### 3.3. Discussion

In this work, it was shown that when either (i) measurement precision is insufficient or (ii) modeling error and measurement uncertainty exceed a problem-specific threshold (lumped into the term

$e_{\text{SDT}}$ ), localized damage is rendered invisible. Moreover, for the purposes of demonstration, it was shown that bounds on the range of  $e_{\text{SDT}}$  may be approximated using a simplified visual method. Of course, in applications where this range is required more precisely, one may utilize Eq. 8 coupled with a search or optimization algorithm. From a practical perspective, however, we are likely interested in increasing the range for which SDT measurements are distinguishable such that small localized damage may be detected. In other words, assuming  $e_p$  is sufficiently low, we are interested in increasing the magnitude of  $e_{\text{SDT}}$  for a given application.

Broadly speaking, this may be accomplished by reducing the error terms using physical and/or computational means. While the totality of such methods cannot be covered in a single article, a few useful strategies are discussed in the following:

- *Increase the sensitivity of the data to changes in the SDT parameter field.* In the case of single-state ERT, for example, this means increasing the sensitivity of  $V$  to changes in  $\sigma$ . This is particularly relevant in large-scale SDT applications, where the sensitivity of ERT is low far from the measuring electrodes. In such cases, one may include (non-boundary) electrodes located within the sensing area, as shown in e.g. [49]. This strategy essentially reduces the ill-posedness of the SDT problem.
- *Approximate modeling errors in  $U$ .* Bayesian approximative error modeling has proven highly successful in reducing errors in cases where low-order modeling is used [29]. In doing this, an approximative error term is incorporated into the inverse problem effectively reducing  $e_m$  and potentially the discretization error  $e_d$ .
- *Data subtraction is effective in reducing systematic errors.* Imaging regimes, such as difference imaging utilize difference data in reconstructing SDT images [50]. As such, a large portion of systematic errors are subtracted. One should note that difference imaging is often qualitative due to linearizing the inverse problem [46].
- *Utilize the proper noise model.* In many SDT cases, the use of Gaussian models is often adequate, for example in constructing the noise covariance matrix  $W$ . In some SDT applications, however, noise may have a Poisson or skew-symmetric distribution [4]. In such applications, the use of a Gaussian model for Poisson/skew-symmetric noise may unnecessarily increase errors due to noise  $e_n$ .
- *Be cautious when selecting the interpolation scheme.* In SDT cases where we aim to map measured data to a grid, such as in elasticity imaging where we map DIC data to a FEM grid, caution should be taken in the interpolation scheme. Often, the use of high-order interpolation schemes (e.g. higher than a cubic order) have been perceived as superior to lower order schemes [51]. As a general statement, this is not true as high order interpolation schemes may result in over fitting [52], thereby incorporating unnecessary interpolation error  $e_I$ .

While these takeaways are of pragmatic significance, it is important to realize that it is difficult to predict the potential for damage visibility and data distinguishability *a priori*. This realization is rooted in the fact that structures are exposed to a plethora of environments and loading conditions, and predicting the extent (or lack) of damage in, e.g. an extreme event can really only be done probabilistically – often with wide ranges of uncertainty [53, 54]. One possible method for circumventing this reality is to incorporate Monte Carlo sampling methods in designing a sensing scheme using simulated – yet realistic – damage processes on the target sensor/structure [55, 56]. This topic will be covered in a future work.

Finally, it is worth remarking that visibility and distinguishability framework proposed and studied herein was realized in the context of SDT. We believe that it can be readily extended to other applied inverse problems, including application areas such as biomedical imaging applications (e.g., magnetic resonance imaging, X-ray tomography, and electrical impedance tomography), industrial process monitoring (e.g., electrical capacitance tomography) and geophysical imaging (e.g. hydraulic tomography and gravitational methods).

#### 4. Conclusions

In this work, we investigated the ever present, yet scarcely examined, topic of damage invisibility and data indistinguishability in the context of structural damage tomography (SDT). Owing to the absence of quantitative criteria for SDT data distinguishability, as it pertains to data sets obtained from undamaged and damaged states, we formulated a damage visibility and data distinguishability criterion for SDT. To demonstrate damage visibility and invisibility, the criterion was applied to an damage detection in an electrically-conductive silver sensing skin using electrical resistance tomography and experimental data. Key realizations and recommendations were provided aiming to improve the ability of SDT regimes to detect nearly invisible damage through the use of the proposed distinguishability criterion.

#### Acknowledgments

DS would like to acknowledge the support of the Civil and Structural Engineering Department at the University of Sheffield. DL was supported by the National Natural Science Foundation of China under Grant No. 61871356 and Anhui Provincial Natural Science foundation under Grant 1708085MA25, this support is greatly acknowledged.

#### References

- [1] Tallman T, Gungor S, Wang K and Bakis C 2015 *Carbon* **95** 485–493
- [2] Cullinan M A and Culpepper M L 2010 *Physical Review B* **82** 115428
- [3] Smyl D, Rashednia R, Seppänen A and Pour-Ghaz M 2017 *Cement and Concrete Research* **91** 61–72
- [4] Smyl D, Bossuyt S, Ahmad W, Vavilov A and Liu D 2019 *Structural Health Monitoring* (in press)
- [5] Tallman T and Hernandez J 2017 *NDT & E International*
- [6] Tallman T, Gungor S, Koo G and Bakis C 2017 *Journal of Intelligent Material Systems and Structures* 1–13
- [7] Hallaji M, Seppänen A and Pour-Ghaz M 2014 *Smart Materials and Structures* **23** 085001
- [8] Hauptmann A, Ikehata M, Itou H and Siltanen S 2018 *Inverse Problems*
- [9] Rattassepp M, Rao J and Fan Z 2018 *NDT & E International* **94** 22–30
- [10] Leong W, Staszewski W, Lee B and Scarpa F 2005 *Smart Materials and Structures* **14** 1387
- [11] Smyl D, Bossuyt S and Liu D 2018 *Journal of Engineering Mechanics* **145** 06018006
- [12] Babaniyi O A, Oberai A A and Barbone P E 2017 *Inverse Problems in Science and Engineering* **25** 326–362
- [13] Antin K N, Harhanen L and Bossuyt S 2016 Damage detection in CFRP components using DIC *Advancement of Optical Methods in Experimental Mechanics (Conference Proceedings of the Society for Experimental Mechanics vol 3)* ed et al J H (Springer) pp 57–62 ISBN 978-3-319-22445-9
- [14] Koohbor B, Mallon S, Kidane A and Sutton M A 2014 *Composites: Part B* **66** 388–399 ISSN 1359-8368
- [15] Aryan P, Kotousov A, Ng C and Cazzolato B 2017 *Structural Control and Health Monitoring* **24** e1894

- [16] Qiang W and Shenfang Y 2009 *Journal of Intelligent Material Systems and Structures* **20** 1663–1673
- [17] Worden K, Farrar C R, Manson G and Park G 2007 *Proceedings of the Royal Society A: Mathematical, Physical and Engineering Sciences* **463** 1639–1664
- [18] Isaacson D 1986 *IEEE transactions on medical imaging* **5** 91–95
- [19] Stefani F, Gundrum T and Gerbeth G 2004 *Physical Review E* **70** 056306
- [20] Birgül Ö, Eyüboğlu B M and Ider Y Z 2003 *Physics in Medicine & Biology* **48** 653
- [21] Mast T D, Nachman A I and Waag R C 1997 *The Journal of the Acoustical Society of America* **102** 715–725
- [22] Adler A and Guardo R 1996 *IEEE transactions on medical imaging* **15** 170–179
- [23] Cheney M and Isaacson D 1992 *IEEE Transactions on Biomedical Engineering* **39** 852–860
- [24] Polydorides N and McCann H 2002 *Measurement Science and Technology* **13** 1862
- [25] Lionheart W R, Kaipio J and McLeod C N 2001 *Physiological measurement* **22** 85
- [26] Jesus A, Brommer P, Westgate R, Koo K, Brownjohn J and Laory I 2019 *Journal of Civil Structural Health Monitoring* 1–15
- [27] Seppänen A, Hallaji M and Pour-Ghaz M 2017 *Structural Health Monitoring* **16** 215–224
- [28] Bhuiyan M Z A, Wang G, Wu J, Cao J, Liu X and Wang T 2017 *IEEE Transactions on Dependable and Secure Computing* **14** 363–376
- [29] Nissinen A, Kolehmainen V and Kaipio J P 2011 *International Journal for Uncertainty Quantification* **1**
- [30] Quarteroni A, Sacco R and Saleri F 2010 *Numerical mathematics* vol 37 (Springer Science & Business Media)
- [31] Greenleaf A, Kurylev Y, Lassas M and Uhlmann G 2009 *Bulletin of the American Mathematical Society* **46** 55–97
- [32] Surana K S and Reddy J 2016 *The Finite Element Method for Boundary Value Problems: Mathematics and Computations* (CRC Press)
- [33] Yeo K, Hwang Y, Liu X and Kalagnanam J 2019 *Computer Methods in Applied Mechanics and Engineering* **347** 1–20
- [34] Ledger P 2012 *Computer Methods in Applied Mechanics and Engineering* **225** 154–176
- [35] Babuška I and Suri M 1987 *ESAIM: Mathematical Modelling and Numerical Analysis* **21** 199–238
- [36] Liu P and Zheng J 2010 *Materials & Design* **31** 3825–3834
- [37] Kaipio J and Somersalo E 2007 *Journal of Computational and Applied Mathematics* **198** 493–504
- [38] Lipponen A, Huttunen J M, Romakkaniemi S, Kokkola H and Kolehmainen V 2018 *SIAM Journal on Scientific Computing* **40** B305–B327
- [39] Passieux J C and Bouclier R 2019 *International Journal for Numerical Methods in Engineering* 1–21
- [40] Hafizi Z and Epaarachchi J 2015 Dynamic response and signal to noise ratio investigation of nir-fbg dynamic sensing system for monitoring thin-walled composite plate *IOP Conference Series: Materials Science and Engineering* vol 100 (IOP Publishing) p 012056
- [41] Zhou Z and Ou J 2005 Development of fbg sensors for structural health monitoring in civil infrastructures *Sensing issues in civil structural health monitoring* (Springer) pp 197–207
- [42] Papakostas T V, Lima J and Lowe M 2002 A large area force sensor for smart skin applications *SENSORS, 2002 IEEE* vol 2 (IEEE) pp 1620–1624
- [43] Clerk A A, Devoret M H, Girvin S M, Marquardt F and Schoelkopf R J 2010 *Reviews of Modern Physics* **82** 1155
- [44] Nordebo S, Dalarsson M, Khodadad D, Müller B, Waldman A D, Becher T, Frerichs I, Sophocleous L, Sjöberg D, Seifnargarhi N *et al.* 2018 *Journal of Physics D: Applied Physics* **51** 205401
- [45] Zadehkoochak M, Blott B, Hames T and George R 1991 *Journal of Physics D: Applied Physics* **24** 1911
- [46] Vauhkonen P, Vauhkonen M, Savolainen T and Kaipio J 1999 *IEEE T. Biomedical Eng.* **46** 1150–1160
- [47] González G, Kolehmainen V and Seppänen A 2017 *Computers & Mathematics with Applications*
- [48] Smyl D, Pour-Ghaz M and Seppänen A 2018 *NDT & E International* **99** 123–133
- [49] Rashetnia R, Alla O K, Gonzalez-Berrios G, Seppanen A and Pour-Ghaz M 2018 *Materials Evaluation*

**76** 1405–1413

- [50] Liu D, Smyl D and Du J 2019 *IEEE transactions on medical imaging* **38** 145–155
- [51] Smyl D, Antin K N, Liu D and Bossuyt S 2018 *Inverse Problems* **34** 124005
- [52] Dierckx P 1981 *IMA Journal of Numerical Analysis* **1** 267–283
- [53] Rinaldi A, Peralta P, Krajcinovic D and Lai Y C 2006 *International journal of fatigue* **28** 1069–1080
- [54] Sohn H, Worden K and Farrar C R 2002 *Journal of intelligent material systems and structures* **13** 561–574
- [55] Kuwatani T, Nagata K, Okada M and Toriumi M 2014 *Physical Review E* **90** 042137
- [56] Kaipio J P, Kolehmainen V, Somersalo E and Vauhkonen M 2000 *Inverse problems* **16** 1487